Optics Communications 407 (2018) 280–284

Contents lists available at ScienceDirect

Optics Communications

journal homepage: www.elsevier.com/locate/optcom

Bi-dimensional empirical mode decomposition based fringe-like pattern suppression in polarization interference imaging spectrometer

Wenyi Ren [a], Qizhi Cao [b], Dan Wu [c], Jiangang Jiang [a,*], Guoan Yang [d], Yingge Xie [a], Guodong Wang [a], Sheqi Zhang [a]

[a] School of Science, Northwest A&F University, Yangling 712100, China
[b] Key Lab. of Environment Change and Resources Use in Beibu Gulf, MOE, Guangxi Teachers Education University, Nanning 530001, China
[c] College of Mechanical and Electronic Engineering, Northwest A&F University, Yangling 712100, China
[d] School of Electronic and Information Engineering, Xi'an Jiaotong University, Xi'an 710049, China

ARTICLE INFO

Keywords:
Fringe analysis
Fourier transform spectrometer
Empirical mode decomposition

ABSTRACT

Many observers using interference imaging spectrometer were plagued by the fringe-like pattern(FP) that occurs for optical wavelengths in red and near-infrared region. It brings us more difficulties in the data processing such as the spectrum calibration, information retrieval, and so on. An adaptive method based on the bi-dimensional empirical mode decomposition was developed to suppress the nonlinear FP in polarization interference imaging spectrometer. The FP and corrected interferogram were separated effectively. Meanwhile, the stripes introduced by CCD mosaic was suppressed. The nonlinear interferogram background removal and the spectrum distortion correction were implemented as well. It provides us an alternative method to adaptively suppress the nonlinear FP without prior experimental data and knowledge. This approach potentially is a powerful tool in the fields of Fourier transform spectroscopy, holographic imaging, optical measurement based on moire fringe, etc.

1. Introduction

Fringe-like pattern (FP) in CCD images occurs due to an interference effect similar to Newton Rings. The production of constructive and destructive interference patterns can cause substantial quantum efficiency variations in back-thinned CCDs as long wavelength light is multiply reflected between the front and back surfaces. FP begins to be an important issue for CCDs when the absorption depth within the silicon becomes comparable to the thickness of the CCD. This occurs for optical wavelengths in red and near-infrared (NIR) region. The light is internally reflected several times before finally being absorbed [1,2]. If the FP is not corrected, it can adversely affect the science derived from the data.

There were many methods proposed to suppress the FP. The approach for the fringe removal option within the widely used *ccdproc* task in IRAF, but this method can considerably over- or under-correct due to the intrinsic variations of the night sky-emission lines, which are not correlated to exposure time [3]. The *ccdproc* task also gives the option of specifying additional scaling factors via image headers, but this requires considerable manual iteration to get a satisfactory result. Howell has proposed a method which uses a neon lamp as a flat field source and produces high signal to noise ratio(SNR) fringe frames to use for defringing an image during the calibration process [4]. An empirical method for the removal of the FP in the spectral domain and the intensity variations in the imaging domain was proposed by Lagerholm to improve the derived results from VIMOS-IFU data [5,6]. However, the empirical method was constructed and tested on data with slowly varying spectral properties. For other types of data, such as with strongly varying background or low intensities (the FP scales with the intensity), a different approach should be preferred. In these cases it may be better to rely on the combination of several exposures thus mimicking the averaging effect. An automatic fringe removal method to the EFOSC images was proposed by Colin [7]. However, the knowledge of the pattern is an essential part of the method. That is, it is not adaptive. In this paper, an adaptive FP suppression method based on bi-dimensional empirical mode decomposition (BEMD) was proposed for the preprocessing of raw data taken by the polarization interference imaging spectrometer (PIIS) [8,9].

* Corresponding author.
E-mail address: renovel@nwsuaf.edu.cn (J. Jiang).

https://doi.org/10.1016/j.optcom.2017.09.071
Received 28 April 2017; Received in revised form 20 September 2017; Accepted 21 September 2017
0030-4018/

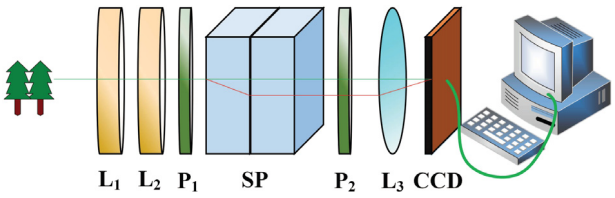

Fig. 1. The schematic of PIIS.

2. Polarization interference imaging spectrometer

PIIS is an imaging spectrometer proposed by Zhang to acquire the spatial and spectral information of the target simultaneously [10,11]. As shown in Fig. 1, the collimating lens is composed by the lenses L_1 and L_2; P_1 is the polarizer; the Savart polariscope, SP, is used as a beamsplitter to split the incident into two rays whose polarization orientation are perpendicular to each other; P_2 is the analyzer; L_3 is the imaging lens; the CCD is placed on the focal plane of L_3; the computer is used to storage and process the raw data. The spatial information can be obtained via realigning the data cube. The spectral information should be retrieved from the realigned interferogram data cube by the fast Fourier transform or other approaches. As shown in Fig. 1, a data cube with the spatial and spectral information could be obtained after the data processing. The raw data taken by the PIIS is the superstition of the image and interferogram which can be taken by the traditional camera and Fourier Transform spectrometer, respectively [12,13]. That is, the spatial and spectral information both are coded in the raw data. PIIS is the combination of the traditional camera and Fourier Transform spectrometer.

The specifications of the PIIS are as follow: the wavelength range is from 480 to 960 nm; the band number is 128; the spectral resolution is 81.4 cm^{-1}; the CCD is produced by Sarnoff Corporation (CAM512, 512×512 pixels, the pixel size is 18 μm×18 μm).

Calibration is a vital and essential procedure during the data processing and information retrieval. During the wavelength and spectral response calibration, the interferogram generated by the monochromatic source must be generated. A back-thinned Sarnoff CCD array is utilized as a detector. If the wavelength is in the red or NIR region, the interferogram would be contaminated by the FP. Consequently, the precise spectrum would not be obtained after the calibration and information retrieval processing.

3. Bi-dimensional empirical mode decomposition

Bi-dimensional empirical mode decomposition (BEMD), a powerful tool for the adaptive and nonlinear image processing, is the extension of empirical mode decomposition (EMD) method proposed by Huang for the nonlinear signal and image processing [14,15]. BEMD has been successfully utilized in pattern recognition, image de-noising, image enhancement, image fusion, etc. [16,17]. In this paper, the raw contaminated images taken by PIIS were decomposed into different intrinsic mode functions (IMFs) which are corresponding to certain content of the image. The sifting procedure of BEMD is implemented by the following steps:

Step 1. Find out all the local maximal and minimal points of the image, respectively;

Step 2. Create the upper and lower envelopes by the spline interpolation of the local maximal and minimal, respectively;

Step 3. For each time, take the mean of the upper and lower envelopes;

Step 4. Subtract the mean image from input image;

Step 5. Check whether the average value of mean image is close enough to zero. If not, repeat the process from step 1 with the result image from step 4 as input image. If it is, the result is IMF, define the residue as result from IMF subtracted from input image;

Step 6. Find out the next IMF by starting over from step 1 with the residue as a new input signal.

4. Fringe-like pattern suppression based on BEMD

According to BEMD, an image $I(x, y)$ can be decomposed into N IMFs and the residue $r(x, y)$ as

$$I(x, y) = \Sigma_{k=1}^{N} IMF_k(x, y) + r(x, y). \quad (1)$$

According to EMD and the properties of the interferogram and FP, we can obtain that:

(1) The frequency of $IMF_k(x, y)$ decreases with its order index k [15];

(2) The monochromatic interferogram is corresponding to the high frequency component of image $I(x, y)$ [18,19];

(3) The FP, which is determined by the structure of CCD, is stable with time and corresponding to the low frequency component of $I(x, y)$ [17–19].

Thereby, the FP, $F(x, y)$, can be reconstructed as

$$F(x, y) = \Sigma_{k=\kappa+1}^{N} IMF_k(x, y) + r(x, y). \quad (2)$$

The reconstructed interferogram, $I_{Rec}(x, y)$, is given by

$$I_{Rec}(x, y) = \Sigma_{k=1}^{\kappa} IMF_k(x, y). \quad (3)$$

The threshold index, κ, is obtained by

$$\Gamma_\kappa \geq \Gamma_{\kappa+1}, \quad (4)$$

where $\Gamma_i = \frac{H(I_{Rec}(x,y))}{H(F(x,y))}$; $H(\cdot)$ is the image information entropy; $I_{Rec}(x, y)$ and $F(x, y)$, respectively, are reconstructed by Eqs. (2) and (3) while $\kappa = i$.

5. Experiment

The contaminated monochromatic interferogram, generated by the source with wavelength of 880 nm, taken by PIIS is shown in Fig. 2(a). The contaminated polychromatic interferogram, generated by a mixtured source of xenon and halogen lamps, is shown in Fig. 2(b). It is obvious that the interferograms had been dramatically distorted by the FP. As shown in Fig. 3, the interferograms shown in Fig. 2(a) and (b) were decomposed into 5 IMFs and the residual via BEMD, respectively. Fig. 3(a) and (g) are the first BIMFs of the interferograms shown in Fig. 2. Fig. 3(f) and (i) are the residuals of the interferograms shown in Fig. 2. As shown in Fig. 3(a) and (l), it was discovered that there are approximately 5 longitudinal and 1 horizontal stripes which are introduced by the CCD mosaic [20]. CCD mosaic, a solution to get a widen-field using the existing CCDs, is to use multiple CCDs to tile the bigger field of view. Some stripes can be found in the original images taken by the mosaic CCD. For example, it has been reported by many researchers [21,22]. Based on their works, the stripes can be both existed in the systems based on the monochromatic and chromatic CCDs. Furthermore, the mosaic stripes were found both the monochromatic and polychromatic interferogram. It can be observed that the interferogram information mostly is coded in the prior IMFs. The FP mainly is coded in the other IMFs and the residuals.

According to the definition of Γ and the decomposition result shown in Fig. 3, the curves of Γ varying with index i were obtained and shown in Fig. 4. κ_m and κ_p, respectively, are the threshold indexes with respect to the monochromatic and polychromatic interferograms. It can be obtained that both the two threshold indexes are 1. Thereby, the interferograms and FPs can be reconstructed based on Eqs. (2) and (3). The reconstructed results were shown in Fig. 5(a)–(d). Fig. 5(a) and (c), respectively, are the reconstructed monochromatic and polychromatic

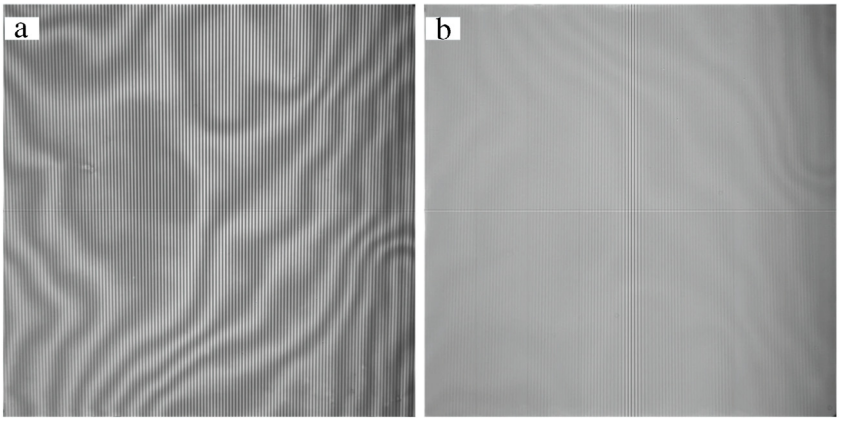

Fig. 2. The monochromatic (a) and polychromatic (b) interferograms contaminated by the FP.

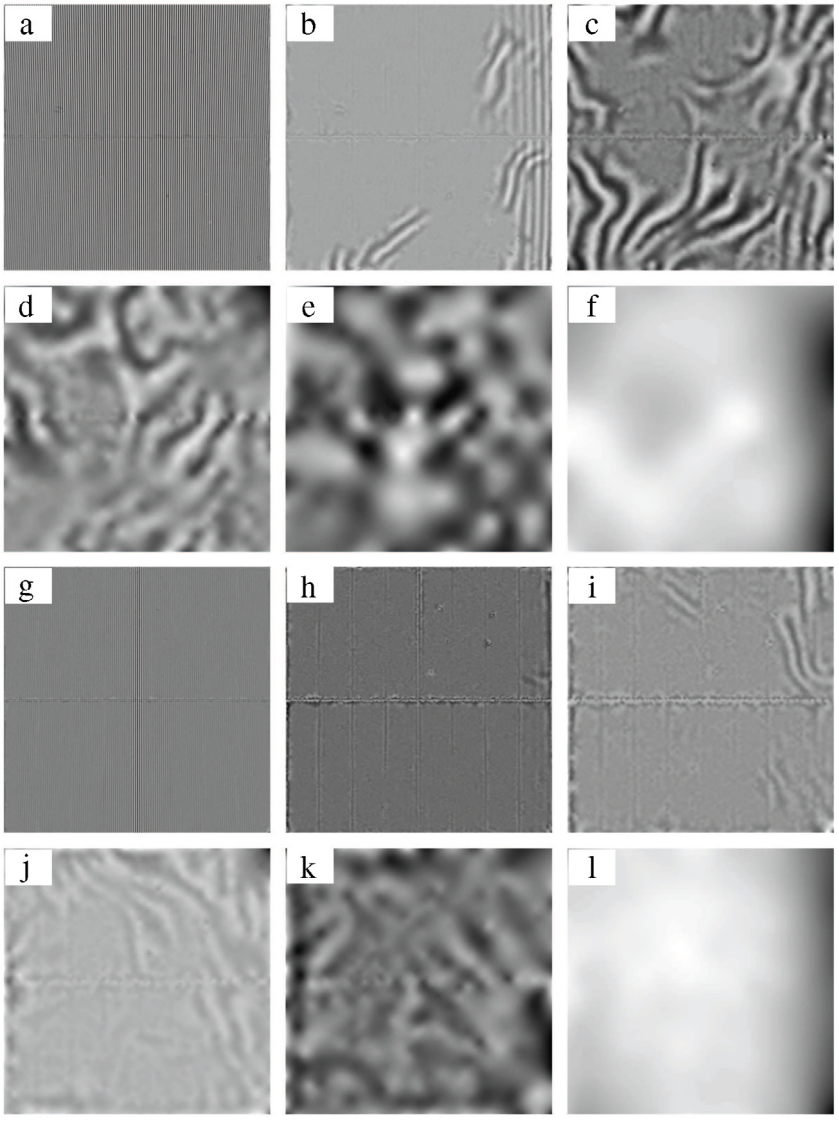

Fig. 3. BEMD of the monochromatic and polychromatic contaminated interferogram: the BIMFs and residual of the monochromatic and polychromatic interferogram, respectively, are shown in figures (a)–(f) and figures (g)–(l).

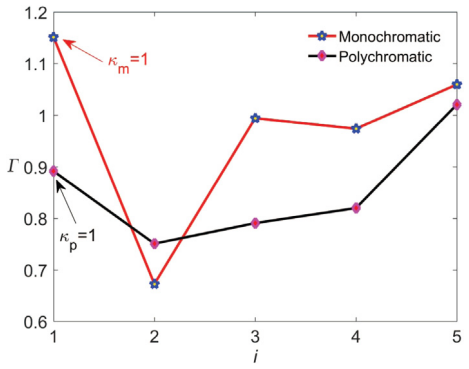

Fig. 4. The variation of Γ with index i.

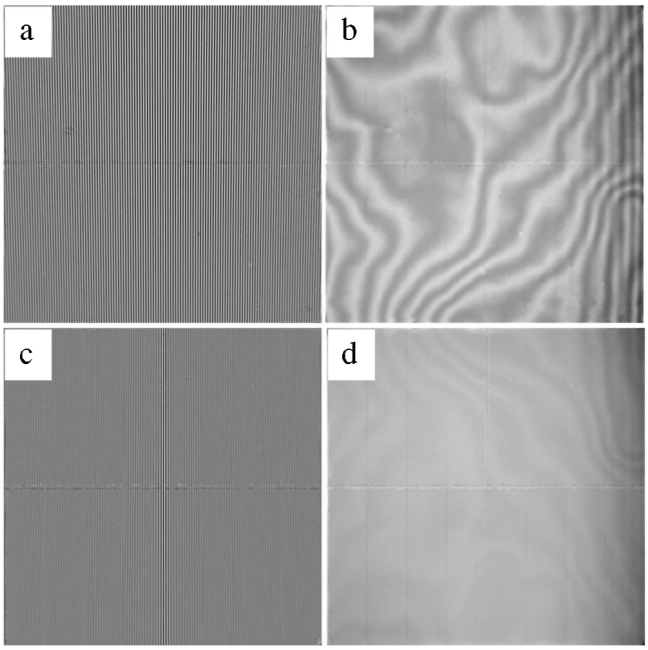

Fig. 5. The reconstructed interferograms and FPs: the reconstructed monochromatic (a) and polychromatic (c) interferograms; the extracted FPs with respect to the monochromatic (b) and polychromatic (d) contaminated interferograms.

interferograms. Fig. 5(b) and (d), respectively, are the extracted FPs from the contaminated monochromatic and polychromatic interferograms. It can be obtained that the FPs were effectively suppressed. Furthermore, the vertical stripes introduced by CCD mosaic were also separated from the interferograms.

According to Fourier transform spectroscopy, the spectrum, $B(\sigma)$, can be retrieved by [18]

$$B(\sigma) = IFT\{I(\Delta)\}, \tag{5}$$

where, $\sigma = 1/\lambda$, is the wavenumber, Δ is the optical path difference, $IFT\{.\}$ is the inverse Fourier transform, $I(\Delta)$ is an one-dimensional (1D) interferogram.

The 100th row of the contaminated interferograms were extracted to evaluate the performance of the FP removal. The extracted FPs, contaminated and corrected interferograms shown in Fig. 6(a) and (c), respectively, are corresponding to the monochromatic and polychromatic interferograms. The green, black and red curves, respectively, denote the contaminated interferogram, corrected interferogram and extracted FP. Where OPD is the abbreviation of optical path difference and D. N. denotes the digital number. It can be found that the asymmetric interferograms are modulated by the nonlinear backgrounds introduced by the FPs. The corrected interferograms are symmetric about the midpoint where OPD is 0. A symmetric interferogram is significant for the phase correction which is an essential processing in spectral information retrieval [23].

Via inverse fast Fourier transform, the spectrums can be retrieved from the interferograms. Thereby, the contaminated and corrected spectrums were retrieved and shown in Fig. 6(b) and (d). The red and blue curves, respectively, denote the contaminated and corrected spectrums. It can be found that there are some sidelobes in the contaminated monochromatic spectrum shown in Fig. 6(b). The sidelobes located in the long wavelength range are introduced by the nonlinear low-frequency background of the interferograms sourced from the FPs. However, the sidelobes located in the short wavelength range are introduced by the noise. To suppress the sidelobes, the background and noise removal processing on the interferogram must be implemented [24]. In addition, it can be obtained that the sidelobes in the long wavelength range (longer than 920 nm) are significantly suppressed in the corrected spectrum. Comparing the contaminated and corrected spectrums shown in Fig. 6(d), it can be discovered that some spurious peaks located in the long wavelength range (longer than 920 nm) were removed in the corrected spectrum. These suppressed peaks were also introduced by the FP. Quantitatively, the SNR of spectrum can be utilized to evaluate the performance of the method. The SNRs of the contaminated monochromatic and polychromatic spectrums, respectively, are 17.15 and 14.92 dB. The SNRs of the corrected monochromatic and polychromatic spectrums, respectively, are 22.53 and 38.57 dB. It can be obtained that the SNR of spectrum was improved after FP suppression. Thereby, the FP suppression can remove the nonlinear background in the interferogram domain and eliminate the spurious peaks located in long wavelength range in the spectrum domain.

6. Conclusion

In summary, an adaptive and nonlinear FP suppression method based on BEMD was proposed for preprocessing the interferogram taken by PIIS. The raw contaminated interferogram is adaptively decomposed into several IMFs and residual firstly. The superstition of the 1st to κth is extracted as the interferogram without FP. The sum of the IMFs from the $(\kappa+1)$th to Nth and the residual is considered as the FP. It was found that the low-frequency background of the interferogram and the sidelobes located in the long wavelength range of the spectrum are suppressed effectively. Comparing with the methods proposed by other researchers, the experimental auxiliary data and priori knowledge are unnecessary in the method. That is, it is an adaptive and nonlinear processing method. By this method, the interferogram can be adaptively extracted from the contaminated interferogram effectively. The background removal processing for the interferogram can be replaced by the FP removal to a certain extent. In addition, the stripes source from the CCD mosaic were suppressed meanwhile. It provides us a significant adaptive preprocessing method for the nonlinear FP suppression in Fourier transform spectroscopy, holographic imaging, and optical measurement based on moire fringe etc.

Acknowledgments

The work is supported by the China Scholarship Council (No. 201706305022), National Natural Science Foundation of China (Nos. 11504297, 61673314, 11664004), Ministry of Science and Technology of the People's Republic of China (No. 2017YFC0403203), Northwest A&F University (Nos. 2452015225, 2452015226, 2452017168, 2452017166, Z109021504, Z109021508), Natural Science Foundation of Shaanxi Province (No. 2016KTZDGY05-02), Guangxi Teachers Education University (No. 2015GXESPKF03).

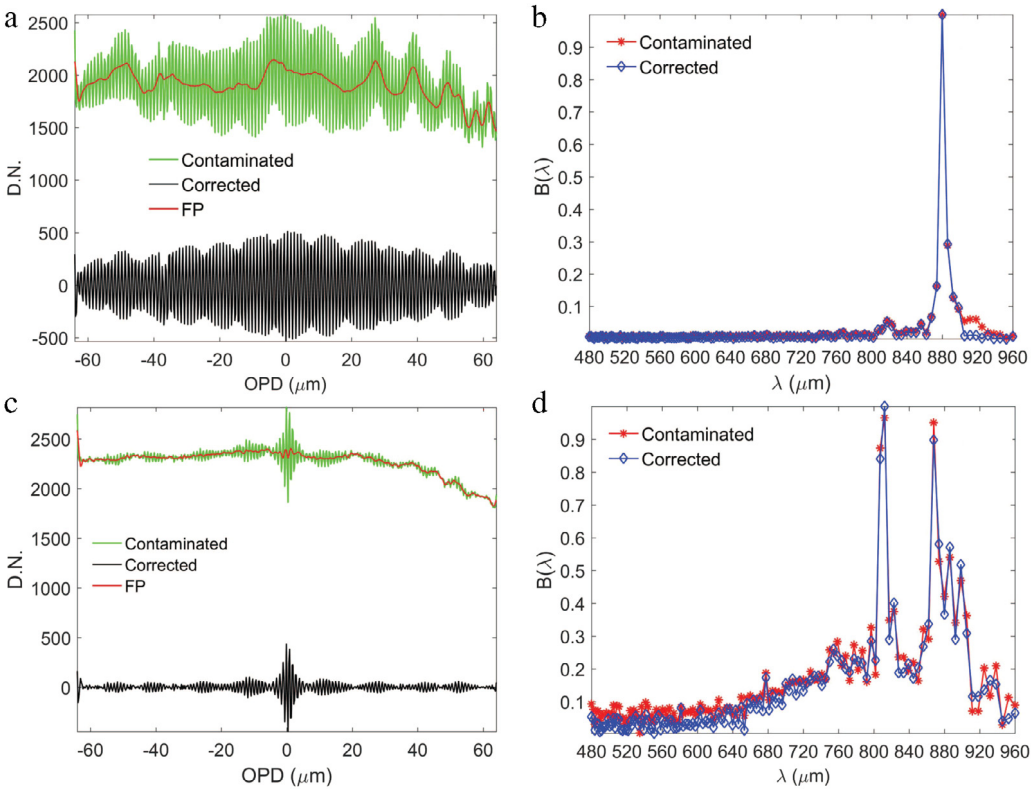

Fig. 6. The FP suppression for the interferograms and their corresponding spectrums: the monochromatic and polychromatic interferograms, respectively, were shown in figures (a) and (c); the monochromatic and polychromatic spectrums, respectively, were shown in figures (b) and (d).

References

[1] M.P. Lesser, E. Olszewski, G.R. Sims, F. Griffin, Optimizing charge-coupled devices for red and near-infrared observations, Proc. SPIE 1071 (1989) (1989) 58–65.

[2] S.B. Howell, Handbook of CCD Astronomy, second ed. Cambridge University Press, Cambridge, 2006.

[3] F. Valdes, The IRAF CCD reduction package, Astron. Data Anal. Softw. Syst. VII (1987) 417–430.

[4] S.B. Howell, Fringe science: defringing ccd images with neon lamp flat fields, Publ. Astron. Soc. Pac. 124 (913) (2012) 263–267.

[5] C. Lagerholm, H. Kuntschner, M. Cappellari, D. Krajnovic, R. Mcdermid, M. Rejkuba, A way to deal with the fringe-like pattern in vimos-ifu data, Astron. Astrophys. 541 (915) (2012) 515–518.

[6] C. Lagerholm, H. Kuntschner, M. Cappellari, D. Krajnovic, R. Mcdermid, M. Rejkuba, A method to deal with the fringe-like pattern in VIMOS-IFU data, Messenger 148 (2012) 17–19.

[7] S. Colin, C. Benoit, Automatic removal of fringes from EFOSC images, Messenger 152 (2013) 14–16.

[8] C. Zhang, B. Xiangli, B. Zhao, Static polarization interference imaging spectrometer (SPIIS), Proc. SPIE 4087 (2000) 957–961.

[9] X. Jian, C. Zhang, L. Zhang, B. Zhao, The data processing of the temporarily and spatially mixed modulated polarization interference imaging spectrometer, Opt. Express 18 (6) (2010) 5674–5680.

[10] X. Jian, C. Zhang, B. Zhao, A new method for spectrum reproduction and interferogram processing, Acta Phys. Sin. 56 (2) (2007) 824–829.

[11] C. Zhang, W. Huang, B. Zhao, Analysis and evaluation on the noise of novel polarization interference imaging spectrometer, Acta Phys. Sin. 59 (8) (2010) 5479–5486.

[12] C. Zhang, X. Jian, Wide-spectrum reconstruction method for a birefringence interference imaging spectrometer, Opt. Lett. 35 (3) (2010) 366–368.

[13] W. Ren, C. Zhang, T. Mu, H. Dai, Spectrum reconstruction based on the constrained optimal linear inverse methods, Opt. Lett. 37 (13) (2012) 2580–2582.

[14] N.E. Huang, Z. Shen, S.R. Long, M.C. Wu, H.H. Shih, Q. Zheng, N. Yen, C.C. Tung, H.H. Liu, The empirical mode decomposition and the hilbert spectrum for nonlinear and non-stationary time series analysis, Proc. Math. Phys. Eng. Sci. 454 (1971) (1998) 903–995.

[15] N.E. Huang, S.R. Long, Z. Shen, A new view of nonlinear water waves: The Hilbert spectrum, Annu. Rev. Fluid Mech. 31 (1) (1999) 417–457.

[16] J.C. Nunes, Y. Bouaoune, E. Delechelle, O. Niang, P. Bunel, Image analysis by bidimensional empirical mode decomposition, Image Vis. Comput. 21 (12) (2003) 1019–1026.

[17] J.C. Nunes, S. Guyot, E. Delechelle, Texture analysis based on local analysis of the bidimensional empirical mode decomposition, Mach. Vis. Appl. 16 (3) (2005) 177–188.

[18] Z. Liu, P. Song, J. Zhang, J. Wang, Bidimensional empirical mode decomposition for the fusion of multispectral and panchromatic images, Int. J. Remote Sens. 28 (18) (2007) 4081–4093.

[19] C. Zhang, W. Ren, T. Mu, L. Fu, L. Jia, Empirical mode decomposition based background removal and de-noising in polarization interference imaging spectrometer, Opt. Express 21 (3) (2013) 2592–2605.

[20] F.G. Valdes, The IRAF mosaic data reduction package, Astron. Data Anal. Softw. Syst. VII 145 (1998) 53–57.

[21] F. MaiaS, A. Piatti, J. Santos, W. Corradi, Basis for a SOAR optical imager pipeline, Bol. Asoc. Argent. Astron. Plata Argent. 54 (2011) 431–434.

[22] K. Lee, A bvr photometric survey of the small magellanic cloud with a mosaic CCD, J. Korean Earth Sci. Soc. 34 (5) (2013) 415–427.

[23] M.L. Forman, W.H. Steel, G.A. Vanasse, Correction of asymmetric interferograms obtained in fourier spectroscopy, JOSA 56 (1) (1966) 59–61.

[24] J.M. Hollas, Modern Spectroscopy, Wiley, 2004.